



# The influence of geometrical parameters on heat and mass transfer processes in rotary heat exchangers

Paulina Kanaś<sup>1</sup> · Andrzej Jedlikowski<sup>1</sup> · Sergey Anisimov<sup>1</sup>

© The Author(s) 2019 **OPEN**

## Abstract

This paper focuses on the influence of geometrical parameters of the rotary heat exchanger on its operation under high-speed rotor conditions. Proposed mathematical model of heat recovery wheel is based on a structure of the counter-flow heat exchanger model. After implementation of a numerical method on the modified  $\alpha$ -model, the computer simulations were conducted. They allowed considering the distribution of the active heat and mass transfer zones (“dry”, “wet” and “frost”) on the matrix channel surface depending on the outdoor air conditions for different variants of rotor size. The obtained results indicate that the increase in the wheel’s depth leads to the increase in temperature effectiveness of heat recovery (from 0.667 to 0.814). Moreover, it was also established that the threshold temperature under which the frost is accumulated on the core surface also rises with the rotor depth (from  $-10.7$  to  $-9.6$  °C). It was concluded that under certain outdoor air temperature conditions ( $t_{1, > -10.7}$  °C, for rotor depth equal to 0.40 m), the mass transfer rate of the condensed water vapor in the channels of the return air side is equal to the evaporation mass transfer rate in the channels of the supply air side, and hence, the temperature efficiency reaches the same value level as under “dry” operating conditions. It was established that only under frost accumulation conditions, the increased temperature effectiveness is observed.

**Keywords** Thermal wheel · Waste heat recovery · Mathematical model · Energy saving

## List of symbols

$c$	Specific heat capacity (J/(kg K))	$L_{X_1}$	Length of heat exchanger channel in $X_1$ direction (m)
$D$	Diameter of the plate channel (m)	$L_{X_2}$	Length of heat exchanger channel in $X_2$ direction (m)
$\Delta \bar{\tau}_1^{\text{evap}}$	Relative duration of the evaporation period of the condensate (dimensionless)	$m$	Water vapor mass flux (kg/(s m <sup>2</sup> ))
$h$	Height of the channel (m)	$M$	Water vapor mass transfer rate (kg/s)
$F$	Heat or heat and mass transfer surface area (m <sup>2</sup> )	$Nu$	Nusselt number (dimensionless)
$F_o$	Total surface area (m <sup>2</sup> )	$n_r$	Rotor speeds (rev/min)
$\bar{F} = (F/F_o) \cdot 100\%$	Heat or heat and mass transfer surface area relates to total surface area (%)	$Pr$	Prandtl number (dimensionless)
$i$	Specific enthalpy (J/kg)	$Re$	Reynolds number (dimensionless)
$Le = \alpha / (\beta c_p)$	Lewis factor (dimensionless)	$t$	Temperature (°C)
$L$	Length of the plate channel (m)	$W$	Heat capacity rate of fluid (W/K)
		$x$	Humidity ratio (kg/kg)

✉ Andrzej Jedlikowski, andrzej.jedlikowski@pwr.edu.pl | <sup>1</sup>Department of Air Conditioning, Heating, Gas Engineering and Air Protection, Faculty of Environmental Engineering, Wrocław University of Science and Technology, 4/6 Norwida st., 50-373 Wrocław, Poland.



SN Applied Sciences (2019) 1:526 | <https://doi.org/10.1007/s42452-019-0540-2>

Received: 31 January 2019 / Accepted: 26 April 2019 / Published online: 6 May 2019

$X$ or $X_1$	Cartesian coordinate in $X$ direction (along outdoor airflow direction) (m)
$\bar{X}_1 = X_1/L_{X_1}$	Relative $X$ coordinate (dimensionless)
$X_2$	Cartesian coordinate in opposite to $X$ direction [m (along return airflow direction)]
$\bar{X}_2 = X_2/L_{X_2}$	Opposite $X$ coordinate (dimensionless)
$\alpha$	Convective heat transfer coefficient ( $W/(m^2 K)$ )
$\beta$	Convective mass transfer coefficient ( $kg/(m^2 s)$ )
$\varepsilon$	Temperature effectiveness of heat exchanger, dimensionless
$\sigma$	Surface wettability factor (0.0...1.0) (dimensionless)

### Subscripts

'	Condition at the airflow/water film or airflow/frost layer interface temperature
1	Outdoor airflow
2	Return airflow
const	Constant
DP	Referenced to dew point temperature
EA	Exhaust air parameters
fr	Frost layer
$g$	Water vapor
$i$	Inlet
max	Maximum value
min	Minimum value
$o$	Outlet
OA	Outdoor air parameters
$p$	Plate surface/under constant pressure conditions
RA	Return air parameters
SA	Supply air parameters
sat	Saturation state
$w$	Water film

### Acronyms

AHU	Air handling unit
HVAC	Heating, ventilation and air conditioning
$NTU = \alpha F / (Gc_p)$	Number of transfer units
RH	Relative humidity

## 1 Introduction

Nowadays, in the era of a big economic development, the significant increase in global energy consumption is observed. The expected development of the building sector, next to the industry and transport, has become responsible for this state. It is estimated that the level of buildings energy use constitutes about 40% of total primary energy consumption in developed countries [1]. Therefore, the legal regulations related to the reduction of energy demand have appeared. In modern buildings, energy is used mostly to ensure the required indoor air parameters [2]. Thermal insulation improvement allows reducing the static heat loss or heating gain in a building. However, due to the stringent indoor air quality requirements, more fresh air has to be supplied using mechanical ventilation systems. It causes an increase in energy demand for ventilation [3]. Energy saving can be achieved by using high-efficiency HVAC systems, including exhaust air heat/energy recovery exchangers. Different types of heat recovery devices such as: fixed-plate exchangers, rotary exchangers, coil energy recovery loops and heat-pipe heat exchangers were compared in ASHRAE Handbook [4]. However, only fixed-plate and rotary heat exchangers have become widespread and are being used by more and more customers.

Thermal wheels constitute a group of the most often used heat recovery exchangers in the HVAC systems in Poland. One of their major advantages is high efficiency exceeding even 80% [5]. The reason for achieving such a high level is the potential to recover not only sensible, but also latent heat. In the case of water vapor condensation in the return airflow channels, this generated moisture can be assimilated by the supply air flowing through the same channel in the next part of the cycle. For similar reasons, many manufacturers produce rotors covered with hygroscopic material, which allows for a more intensive heat and mass exchange between two airflows. Such devices are called energy wheels.

In order to analyze the effectiveness of rotary heat exchanger, their construction and working principles should be presented. The rotary heat exchanger (Fig. 1) consists of a rotor made of 0.06–0.10 mm thick aluminum foils [6], which constitute a storage mass. Alternately wrapped wavy and straight tapes (sheets) form a large number of small axially arranged channels through which both airstreams flow. The height of these channels varies from 1.4 to 2.7 mm [6, 7]. As the wheel matrix rotates with specified speed between two air channels (supply and return), it transfers the heat from warmer to cooler airflow. The rotation is caused by the electric

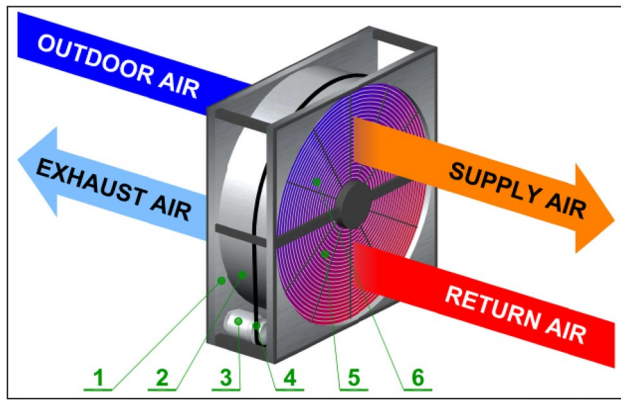


**Fig. 1** Heat recovery section with a rotary heat exchanger: 1—metal housing, 2—rotor, 3—electric motor, 4—drive belt, 5—return air side, 6—supply air side

motor with belt pulley and v-belt connected to the rotor. The whole construction is fitted in a metal housing.

In winter, the warm and humid exhausted air passes through one half of the matrix, transmitting the majority of its heat to the storage mass, while the cold and dry outdoor air flows through the other half and receives heat accumulated in the previous part of the revolution. This cycle repeats as long as the wheel rotates.

Potential of air-to-air heat recovery exchangers has caused them to be the subject of many considerable and detailed studies. For many years, researchers have considered the correct operation of heat exchanger. There are a lot of research papers including analysis of heat transfer processes (under dry and phase transition conditions) [8–12]. In addition, many authors analyzed also the influence of different thermodynamic and geometrical parameters on heat recovery efficiency. In order to effectively predict the behavior of these heat exchangers under different climatic conditions, several numerical methods were developed. The researchers have also raised the issue of freezing problem.

Justo Alonso et al. [13] emphasized the need for using mechanical ventilation systems with heat recovery devices while designing Zero Energy Building in cold climate. They focused on comparison of the properties for different types of heat/energy recovery systems: recuperative and regenerative heat exchangers and also regenerative energy exchangers. Both heat and energy wheels are more susceptible to air leakage than recuperators since the latter ones have both air streams separated. At the same time, they concluded that heat wheels are characterized by lower risk of frosting than the flat-plate heat exchangers. The researchers also presented a variety of methods that allow determining the sensible and latent effectiveness of the rotary heat/energy exchanges. Fathieh et al. [14] analyzed the possibility to predict sensible

effectiveness of air-to-air heat wheel on the basis of cyclic and single-step change transient experiments performed on the parallel-plate heat exchanger made of the same material. Their results indicated that this method may be successfully used to determine the sensible effectiveness of the parallel-flow rotors. In the case of counter-flow wheels, predicted values differed from the real efficiency, which made this method unreliable. In papers written by Abe et al. [15, 16], the analytical model for estimating the effectiveness of energy wheel was also developed. The model uses the characteristics measured on the same non-rotating wheel operating under a step change in temperature and humidity. Then the predicted results of the sensible and latent effectiveness were compared with the experimental standard test data and the numerical simulation results achieving agreement within the uncertainty boundary. Another study [17, 18] shows correlations which may be used to determine sensible, latent and total effectiveness of energy wheel on the basis of known operating conditions. The presented equations use the dimensionless group for heat and moisture transfer. Simulation data confirmed the reliability of these correlations. Seo et al. [19] described a simple model which allows receiving the effectiveness of heat wheels with a maximum error of 5% within a wide range of rotational speed. It was based on the governing equations of a periodic-flow heat exchanger. They indicated that this method is very useful in practical applications.

The researchers have also developed many theoretical models of heat exchangers to investigate heat and mass transfer processes in detail as well as the impact of different physical and thermophysical parameters on the heat recovery efficiency. Büyükalaca and Yilmaz discussed the influence of rotational speed on the effectiveness of rotary heat exchangers [20]. The authors focused especially on low-speed operating conditions. As a result of their numerical and experimental studies, an empirical equation to calculate the effectiveness at low values of rotational speed was obtained. The authors also proved that the empirical equation of Kays and London [21] is not valid in the case of low-speed region. Nizovtsev et al. [10] studied the processes of condensation and vaporization in the regenerative air-to-air heat exchanger with periodic change in the air flow direction. For this purpose, the physical and mathematical model was developed. The authors analyzed the influence of relative humidity of the rooms on heat and mass transfer processes. They paid particular attention to the three characteristic entire indoor RH ranges that differed in moisture transfer processes ( $RH < 30\%$ ,  $RH = 30 \dots 80\%$ ,  $RH > 80\%$ ). In the first range of relative humidity, there is no mass transfer. The second range of indoor RH is characterized by balanced condensation and vaporization processes, while

the moisture accumulation in the channels can only be observed in the third range of RH. The analysis of the influence of relative humidity is a very important issue of the operation of rotary heat exchanger. This makes it possible to determine the conditions responsible for freezing processes. Frost formation on the plate surface of the air-to-air heat exchangers is a common problem leading to the decreasing performance of heat recovery systems operating in cold climates. In the past three decades, a number of researchers have sought to determine the operating conditions which frost can occur inside the heat/energy exchangers.

A lot of papers also contain the analysis of frost control strategies and defrosting methods. For example, in 1989 Holmberg [9] analyzed frosting limit in both non-hygroscopic and hygroscopic surfaces of energy wheels. In the case of non-hygroscopic rotary heat exchanger, the core was made of untreated aluminum. Hygroscopic exchanger was additionally covered by an oxide layer. The results showed that frosting limit of a hygroscopic wheel is even 10 °C lower than the limit of non-hygroscopic rotor. Laboratory tests also showed that it took twice more time to cause 50% increase in pressure drop while operating non-hygroscopic wheel. Ten years later, Bilodeau et al. [22] investigated freezing in the rotary heat and mass exchanger. Experimental part of their studies evidenced that glazed frost dominates over rough frost in these types of exchangers. They also developed the transient three-dimensional model, which allowed indicating that the absolute humidity of the exhaust air is the most important parameter determining the frost formation. Additionally, they showed nonlinear variation of the AH (absolute humidity) and the temperature of the air streams flowing through the frost zone. The authors also made a conclusion that the traditional frost control strategies should be replaced by the new ones to improve the performance of the heat recovery systems. Nasr et al. [23] raised the issues of frost formation and freeze protection methods in air-to-air heat and energy exchangers. For this purpose, a detailed literature review was conducted. On its basis, it may be noticed that the problem of frost formation was studied mostly for flat-plate heat exchangers. Moreover, their paper also contains the comparison of the different frost control strategies and defrosting techniques including capital and operating costs. The authors added that the problem of frost formation had been a subject of studies for over 30 years; however, they stressed the need for more detailed researches, especially in the field of frost accumulation on surfaces of both rotary and flat-plate exchangers.

In recent years, several attempts have been made to determine the frosting limits. Anisimov et al. [11] performed the simulation based on the mathematical model

to investigate both heat and mass transfer processes in a cross-flow exchanger operating under frost conditions. The influence of the relative humidity of return air on the temperature effectiveness has been proven—the increase in the effectiveness with increasing RH is a result of the effect of heat of phase transition. The authors also proposed safe operating conditions for different performances of the considered heat exchanger. Moreover, they noticed that the return air parameters with the value of dew point temperature equaled 0 °C are the variants with the most unfavorable threshold temperatures. Jedlikowski et al. [12] presented a modified  $\alpha$ -model, which allows analyzing the heat and mass transfer processes inside a counter-flow heat exchanger. It was underlined that the formation of different heat and mass transfer regions depends mostly on the relative humidity of exhaust air and outdoor air temperature. The authors focused on the frost formation phenomenon and presented frost threshold temperatures for various operating conditions, on the basis of which the analysis of optimal bypass frost control strategies was conducted. Moreover, it was noticed that even the fully opened bypass damper is not a sufficient method under some sub-zero outside air temperature operating conditions. A continuation of the topic of frost protection methods for a counter-flow heat exchanger can be found in other paper [24]. Pacak et al. conducted the analysis of power demand for two commonly used techniques: bypassing and preheating the outdoor airflow. Their investigation was based on a theoretical model and examined for different return air parameters and values of heat exchanger effectiveness. The results revealed that preheating is characterized by higher heat recovery efficiency within the most typical return airflow conditions and lower total power demand. In the paper written by Liu et al. [25], the frost formation problem in both cross-flow heat and energy exchangers was presented. The aim of this research was therefore to determine the frosting limits and analyze the impact of operating parameters on these limits. Another important practical information was defining the sensible and latent effectiveness for the energy exchanger to avoid frosting. Liu et al. [26] constructed and tested a prototype of a novel air-to-air quasi-counter-flow membrane heat exchanger. The analysis concerned heat and moisture transfer for low operating temperatures. For this purpose, the analytical model was developed. The heat exchanger reached a high sensible and latent effectiveness. This study also showed that the effectiveness level does not depend on the outside air temperature as long as there is no condensation and frost. The third paper of the authors [27] comprised a model, which allowed defining the frost threshold temperature.

The literature review allows drawing the conclusion that recently the most widely studied devices are the

fixed-plate heat exchangers (both counter-flow and cross-flow) and the enthalpy rotary wheels. However, far too little attention has been paid to the non-hygroscopic wheels. In this paper, the influence of geometrical parameters on heat and mass transfer processes and effectiveness of rotary heat exchanger is presented.

## 2 Theoretical analysis of heat and mass transfer process

The possibilities of creating different areas of active heat and mass transfer inside the rotary heat exchanger require thorough analysis of its operation (Fig. 2). One of the most frequently considered cases of year-round operation of heat exchangers under high-speed rotor conditions is the variant of "dry" heat exchange. During such operation, only "dry" heat exchange takes place in the channels of heat exchanger as a result of which both sides of the airflow channels remain dry. This situation occurs mainly during the summer. The processes of heat exchange during the cold season (especially in winter) are completely different. Particularly noteworthy are the conditions of extremely low ambient air temperatures. The high temperature difference between the two airflows results in a significant reduction in the plates surface temperature of the heat exchanger. If the temperature of the plate surface is higher than the dew point, the "dry" heat exchange mode takes place ( $\bar{X}_2 = 0.00 \dots 0.34$ ). But, if the temperature of the plate surface is lower than the dew point, the condensation process begins, as a result of which an additional

water film may be formed ( $\bar{X}_2 = 0.34 \dots 0.61$ ). However, if the plate surface temperature additionally drops below the freezing point, the condensed water will gradually freeze ( $\bar{X}_2 = 0.61 \dots 1.00$ ). It is worth noting that the water vapor condensation processes are accompanied by sensible and latent heat transfer. In this way, not only sensible but also latent heat can be recovered. An important problem connected with the operation of these heat exchangers is the danger of freezing the accumulated condensate, which can cause an increase in pressure drop and consequently block the air flow through the heat exchanger. Moreover, during the analysis of the active heat and mass transfer zones creation, it is also worth mentioning the possibility of formation of the so-called "transient" area between "wet" and "frost" areas ( $\bar{X}_2 = 0.61 \dots 0.73$ ). The presence of this area results from the fact that there are parts of surfaces covered with water film and frost layer. A detailed discussion of this phenomenon is presented in our earlier papers [11, 12, 24, 28].

The possibility of creating different heat and mass transfer areas depends on the value of plate surface temperature in relation to the dew point and freezing point temperatures. The conditions for the formation of the three main zones are summarized in Table 1.

The convection heat transfer coefficients for "dry" heat exchange conditions and for some "wet" heat exchange cases can be calculated on the basis of the Nusselt number with uniform heat flux for both thermal entrance region and fully developed flow. Two air streams are considered to be laminar flow [28], due to the low airflow velocity ( $Re < 2000$ ). In this case, the Nusselt number of air can be divided into two areas: the beginning undeveloped region ( $L \leq l_b$ ) and for the fully developed region ( $L > l_b$ ). The length of the first undeveloped zone can be calculated from Eq. (1):

$$l_b / D = 0.05 Re_D Pr \tag{1}$$

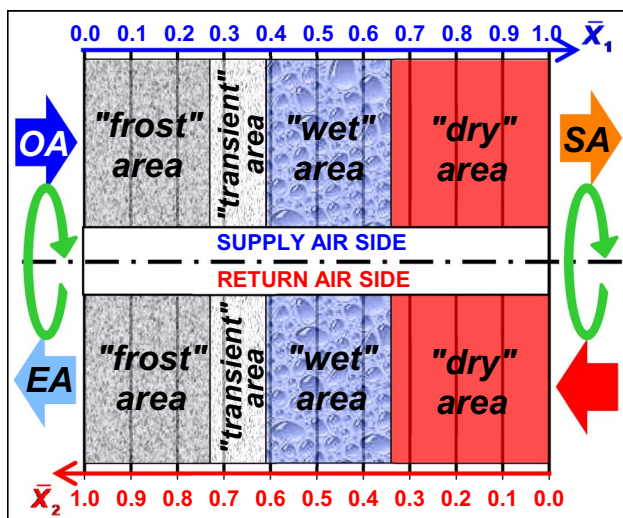


Fig. 2 Schematic diagram of the rotary heat exchanger supplemented with different variants of heat and mass transfer (EA exhaust air parameters, OA outdoor air parameters, RA return air parameters; SA supply air parameters)

Table 1 Conditions for the formation of the three main heat and mass transfer areas

Graphic symbol	Plate surface temperature conditions
	$t_{2i}^{DP} < t_{p2}^{min}$
	$t_{2i}^{DP} < t_{p2}^{max}$ $0^\circ C < t_{p2}^{min} < t_2^{DP}$
	$0^\circ C < t_{p2}^{max} < t_{2i}^{DP}$ $t_{p2}^{min} < 0^\circ C < t_2^{DP} \cup t_{p2}^{min} < t_2^{DP} < 0^\circ C$ $t_{p2}^{max} < 0^\circ C < t_{2i}^{DP} \cup t_{p2}^{max} < t_{2i}^{DP} < 0^\circ C$

For the first area, the Nusselt number can be determined by means of empirical Eqs. (2) or (3), depending on the boundary conditions [28]:

$$Nu_h^{I,cond} = 1.533 [Re_h Pr(h/L)]^{1/3} \tag{2}$$

$$Nu_h^{II,cond} = 1.755 [Re_h Pr(h/L)]^{1/3} \tag{3}$$

For the fully developed air flow region, the Nusselt number is constant [29–31]. For the flat channel:

$$Nu_h^{I,cond} = 3.77 \tag{4}$$

$$Nu_h^{II,cond} = 4.12 \tag{5}$$

In the case of sine passage [29–37]:

$$Nu_h^{I,cond} = 2.39 \tag{6}$$

$$Nu_h^{II,cond} = 3.014 \tag{7}$$

In the case of triangular passage [29–37]:

$$Nu_h^{I,cond} = 2.47 \tag{8}$$

$$Nu_h^{II,cond} = 3.111 \tag{9}$$

Calculations of local values of Nusselt numbers were carried out taking into account the variable height of the channel caused by the variable thickness of frost.

### 3 Description of the mathematical model

The mathematical model of rotary heat exchanger is based on the structure of the counter-flow heat exchanger model [12, 24]. Depending on the value of rotor speed or solid-to-airflow heat capacity rate ratio, the effectiveness of the heat recovery depends on the two characteristic operating states: high speed (non-oscillation mode) and low speed (oscillation mode). For the values of rotating speed lower than the critical speed  $n_r < n_r^{critical}$ , the plate surface temperature will oscillate. A gradual decrease in rotor speed will therefore increase the amplitude of the plate surface temperature oscillation. Increasing the amplitude of the plate surface temperature oscillation reduces the driving force of the heat exchange processes, which in turn reduces the heat exchanger effectiveness [19, 29]. Analyzing the influence of rotational speed on the heat transfer process, Kays and London proposed the empirical correlation to determine the rotary heat exchanger effectiveness with a compliance rate of  $\pm 1\%$  [21]:

$$\varepsilon = \varepsilon_o \phi \tag{10}$$

where  $\varepsilon_o$  temperature effectiveness of the counter-flow heat exchanger,  $\phi$  correction factor for rotational speed.

The correction factor for rotational speed can be determined by the following equation [21]:

$$\phi = \left( 1 - 9 / \overline{W}_r^2 \right) \tag{11}$$

where  $\overline{W}_r$  solid-to-airflow heat capacity rate ratio.

The solid-to-airflow heat capacity rate ratio can be calculated by means of the formula:

$$\overline{W}_r = W_r / W_1 \tag{12}$$

where  $W_r$  solid heat capacity rate,  $W_1$  supply airflow heat capacity rate.

A similar formula, in agreement with the data presented by Kays and London, has been proposed by Büyükalaca and Yilmaz [20, 38]:

$$\varepsilon = \frac{\overline{W}_r}{\left[ 1 + 3 \left( \overline{W}_r / \varepsilon_o \right)^2 + \left( \overline{W}_r / \varepsilon_o \right)^4 \right]^{1/4}} \tag{13}$$

It should be noted that in the case of periodic steady-state operation, the plate surface temperatures in the direction of air flow are similar to temperatures determined for the channels of the counter-flow heat exchanger.

However, an increase in rotational speed above the critical value  $n_r > n_r^{critical} \approx 5 \text{ rev/min}$  [29].

( $\overline{W}_r > \overline{W}_r^{critical} \approx 5$  [19, 20, 29]) has practically no effect on the temperature effectiveness of the heat exchanger. In this case, the local temperature of plate surface in each cross section of the rotor remains practically constant during rotor rotation ( $t_{p1} \approx t_{p2} \approx t_p$ ). For this reason, the temperature profile of matrix in the direction of air flow would be similar to the temperature profile of the counter-flow heat exchanger with temperature effectiveness  $\varepsilon_o$ .

Based on the main assumptions described above for the operation of the rotary heat exchanger under non-oscillating conditions, the basic equation for high rotor speeds  $n_r > n_r^{critical}$  can be significantly simplified and presented as simple differential equations of the heat and mass balance developed for supply and return airflows with a first-order solution.

The proposed modified  $\alpha$ -model of the rotary heat exchanger is considered according to the system of coordinates  $X_1$  (outdoor airflow direction) and  $X_2$  (return airflow direction) (Fig. 2). In order to simplify the structure

of model, a number of basic assumptions were introduced, including those based on models available in the published papers [11, 12, 24, 28]:

- The heat exchanger operates in quasi-steady-state conditions.
- The outdoor and return airflows in contact with the plate surface are treated as an ideal, homogeneous and incompressible gas.
- The driving force of the mass exchange process is the moisture content gradient.
- The heat and mass transfer inside the rotor matrix take place in the normal direction ( $\alpha$ -model [29, 30]).
- There are no additional heat sources in the airflows.
- Water vapor condensation may initially form on the part of plate surface located on the return air side (semi-circular geometry), and then as a result of rotor rotation, the condensate will be transferred to the outdoor air section.
- The evaporated heat flux may in no case be greater than the heat of water vapor condensation.
- The temperature of the airflows varies according to the directions of the coordinate system.
- Heat losses to the ambient air are ignored.

On the basis of the above-mentioned assumptions, the equations of balances for the outdoor and return airflow and for the matrix of the rotary heat exchanger were developed.

Energy balance for the outdoor and return air streams under "dry" heat transfer conditions can be expressed as follows:

$$\frac{dt_1}{d\bar{X}_1} = NTU_1(t_{p1} - t_1) \tag{14}$$

$$\frac{dt_2}{d\bar{X}_2} = NTU_2(t_{p2} - t_2) \tag{15}$$

$$\left(\frac{W_1}{W_2}\right) \frac{dt_1}{d\bar{X}_1} + \frac{dt_2}{d\bar{X}_2} = 0 \tag{16}$$

In this case, only sensible heat transfer takes place inside the channels of rotary heat exchanger so that the moisture content of both air streams will be constant and unchanged ( $x_1 = \text{const}$ ) and ( $x_2 = \text{const}$ ).

The set of equations for heat exchange processes under water vapor condensation conditions is much more complicated. In such case, the sensible and latent heat transfer may occur at the same time. For this reason, temperature

changes will also be accompanied by changes in the moisture content of the air stream.

Mass balance for the return and outdoor air streams under water vapor condensation conditions can be presented in the form:

$$\frac{dx_2}{d\bar{X}_2} = NTU_2 \left(\frac{\sigma_p}{Le}\right)_2 (x'_{p2} - x_2) \tag{17}$$

$$\frac{dx_1}{d\bar{X}_1} = NTU_1 \left(\frac{\sigma_p}{Le}\right)_1 (x'_{p1} - x_1) \Delta\bar{\tau}_1^{\text{evap}} \tag{18}$$

The component  $\Delta\bar{\tau}_1^{\text{evap}}$  in Eq. (18) means the relative duration of the evaporation period of the condensed water film (or frost sublimation) in the outdoor air flow section. It is worth mentioning that this component refers to the condition from the model assumptions concerning the possibility of water evaporation (or frost sublimation) in an amount not exceeding the evaporating mass flow rate from the return air channel.

The relative duration of the evaporation period of the condensate can be calculated by means of a set of equations:

$$\begin{cases} \Delta\bar{\tau}_1^{\text{evap}} = m_2/m_1, & \text{if } m_2 \leq m_1 \\ \Delta\bar{\tau}_1^{\text{evap}} = 1.0, & \text{if } m_2 > m_1 \end{cases} \tag{19}$$

Water vapor mass flux on the matrix surface for return  $m_2$  and outdoor  $m_1$  air channel necessary for determining the relative duration of the evaporation period of the condensate can be calculated as follows:

$$m_2 = \beta_2 \sigma_{p2} (x_2 - x'_{p2}) = \left(\frac{\alpha \sigma_p}{Le c_p}\right)_2 (x_2 - x'_{p2}) \tag{20}$$

$$m_1 = \beta_1 \sigma_{p1} (x'_{p1} - x_1) = \left(\frac{\alpha \sigma_p}{Le c_p}\right)_1 (x'_{p1} - x_1) \tag{21}$$

It should be noted that if the water vapor mass flow rate in the return air channel exceeds the water vapor mass flow rate in the outdoor air channel, a gradual accumulation of water film or frost layer can be observed on the matrix surface. Such operating conditions of the heat exchanger can be very dangerous, especially when the outdoor air temperature is below freezing. In this case, there is a high risk of frost formation inside the heat exchanger passages, which reduces the effectiveness of the unit and increases the pressure drop in the airflow channels as a result of blockage by frost [11, 12, 28].

Energy balance for the outdoor and return air streams under water vapor condensation conditions can be presented as follows:

$$\frac{dt_2}{d\bar{X}_2} = NTU_2(t'_{p2} - t_2) \tag{22}$$

$$\frac{dt_1}{d\bar{X}_1} = NTU_1(t'_{p1} - t_1) \left[ 1 + \left(\frac{\sigma_p}{Le}\right)_1 \left(\frac{c_g}{c_p}\right)_1 (x'_{p1} - x_1) \Delta \bar{\tau}_1^{evap} \right] \tag{23}$$

- for the case of “wet” heat exchange

$$\left(\frac{W_1}{W_2}\right) \left[ \left(\frac{dt_1}{d\bar{X}_1}\right) + \left(\frac{i_{g1} - i_{w1}}{c_{p1}}\right) \left(\frac{dx_1}{d\bar{X}_1}\right) \right] + \left[ \left(\frac{dt_2}{d\bar{X}_2}\right) + \left(\frac{i_{g2} - i_{w2}}{c_{p2}}\right) \left(\frac{dx_2}{d\bar{X}_2}\right) \right] = 0 \tag{24}$$

- for the case of “frost” heat exchange

$$\left(\frac{W_1}{W_2}\right) \left[ \left(\frac{dt_1}{d\bar{X}_1}\right) + \left(\frac{i_{g1} - i_{fr1}}{c_{p1}}\right) \left(\frac{dx_1}{d\bar{X}_1}\right) \right] + \left[ \left(\frac{dt_2}{d\bar{X}_2}\right) + \left(\frac{i_{g2} - i_{fr2}}{c_{p2}}\right) \left(\frac{dx_2}{d\bar{X}_2}\right) \right] = 0 \tag{25}$$

The solution of the presented sets of simultaneous differential Eqs. (14)–(18) and (22)–(25) requires the introduction of inlet airflow conditions at the entrances to the outdoor and return airflow passages (Fig. 2)

$$t_1 \Big|_{\bar{X}_1=0} = t_{1i} \quad x_1 \Big|_{\bar{X}_1=0} = x_{1i} \quad t_2 \Big|_{\bar{X}_2=0} = t_{2i} \quad x_2 \Big|_{\bar{X}_2=0} = x_{2i} \tag{26}$$

$$\bar{X}_2 = 1.0 - \bar{X}_1 \tag{27}$$

and boundary conditions for supply and exhaust air side matrix surface:

$$\begin{aligned} \sigma_{p2} \Big|_{t_{p2} > t_2^{DP}} = 0 & \quad \sigma_{p1} \Big|_{t_{p1} = t_{p2} > t_2^{DP}} = 0 \\ \sigma_{p2} \Big|_{t_{p2} \leq t_2^{DP}} = 1 & \quad \sigma_{p1} \Big|_{t_{p1} = t_{p2} \leq t_2^{DP}} = 1 \\ x'_{p2} \Big|_{0^\circ\text{C} < t_{p2} \leq t_2^{DP}} = x_{p2}^{sat} & \quad x'_{p1} \Big|_{0^\circ\text{C} < t_{p1} = t_{p2} \leq t_2^{DP}} = x_{p1}^{sat} \\ x'_{p2} \Big|_{t_{p2} < t_2^{DP} \cap t_{p2} < 0^\circ\text{C}} = x_{fr2} \Big|_{Z_2=\delta_{fr2}} & \quad x'_{p1} \Big|_{t_{p1} = t_{p2} < t_2^{DP} \cap t_{p1} = t_{p2} < 0^\circ\text{C}} = x_{fr1} \Big|_{Z_1=\delta_{fr1}} \end{aligned} \tag{28}$$

The presented sets of equations describing the heat and mass exchange in the matrix of the rotary heat exchanger are nonlinear and cannot be solved using analytical methods. For this reason, it was decided to use numerical methods based on the modified Runge–Kutta

method. This method has an adequate accuracy and stability, which has been confirmed by solving similar problems [11, 12, 24, 28, 39–41].

### 4 Mathematical model validation

In order to validate the mathematical model of the rotary heat exchanger, a test stand was built (Fig. 3) [40]. The stand is equipped with the following devices and components: air intake, air outlet, duct filter, piping and air ducts, electrical cables and other components, axial fan (manufacturer Rosenberg), rotary heat exchanger (model RRU PT-D19-W-715, manufacturer Klingenburg), duct heater (manufacturer Systemair), duct air conditioner used as an air cooler (manufacturer Fujitsu), control dampers and non-return flaps. Polycarbonate probes with TH200 transmitters were used to test the operation of the heat exchanger (manufacturer KIMO Instruments, with 0.2 °C temperature and 3% relative humidity accuracy). To determine the volume flow rate, TROX Technik’s VMR Ø315 units were used (accuracy of measurement 5%). A computer and software provided by Kimo Instruments were used to record the system’s performance.

The model validation was carried out by comparing the results of measurements and numerical simulations of exchanger operation performed for the same air parameters (Fig. 4). The results of the comparison are presented in the form of the changes in supply air temperature expressed as a function of the outdoor air temperature for the air flow rate of 500 m<sup>3</sup>/h. As one can see, deviations between the results of measurement and simulation are in the range – 10... + 14%. The visible slight differences are mainly due to non-uniform airflows distribution, system

leakage and heat losses. The presence of frost was determined on the basis of measurements of pressure drops in the heat recovery system, causing an increase in resistance to flow through the exchanger. Good agreement of experimental and simulation results confirms the adequacy of



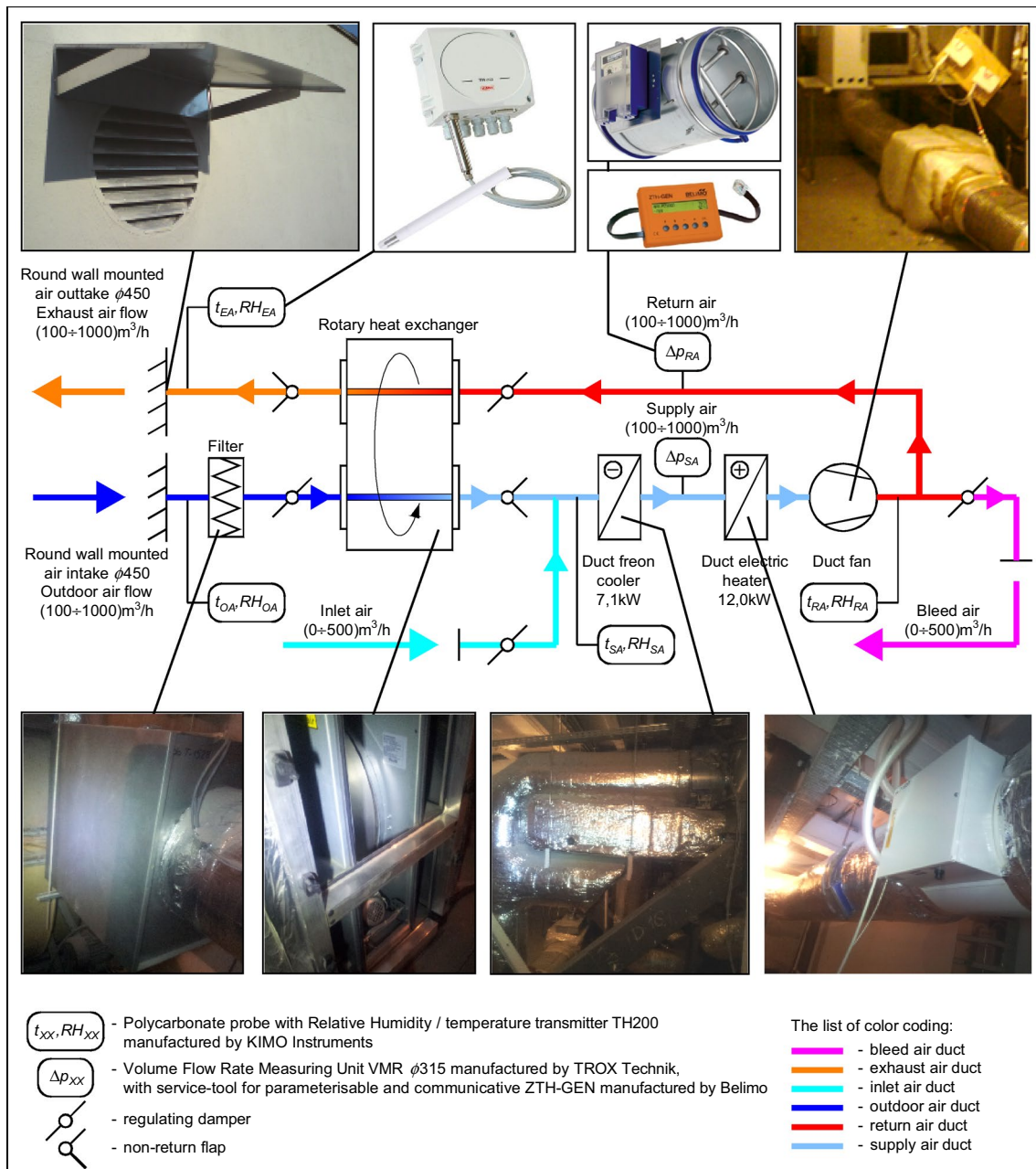


**Fig. 3** Schematic diagram of the testing stand supplemented with selected photographs (EA exhaust air parameters, OA outdoor air parameters, RA return air parameters; SA supply air parameters)

the developed model, so it can be concluded that the mathematical model allows to effectively predict the efficiency of rotary heat exchanger operation.

### 5 Results of simulations

Simulations were carried out at fixed geometrical parameters (wheel diameter 0.715 m, housing height 0.800 m, housing width 0.900 m) and five different variants of a

rotor depth: 0.20, 0.25, 0.30, 0.35 and 0.40 m, assuming constant parameters of return air ( $t_{ri} = 20 \text{ }^\circ\text{C}$ ,  $RH_{2i} = 40\%$ ) and variable outdoor air temperature. The values of outdoor air temperatures were chosen in such a way that it was possible to separate the boundaries of formation of different active heat and mass transfer zones. The received results allowed analyzing the heat and mass transfer processes as well as their influence on temperature effectiveness of the rotary heat exchanger. The effects of simulation

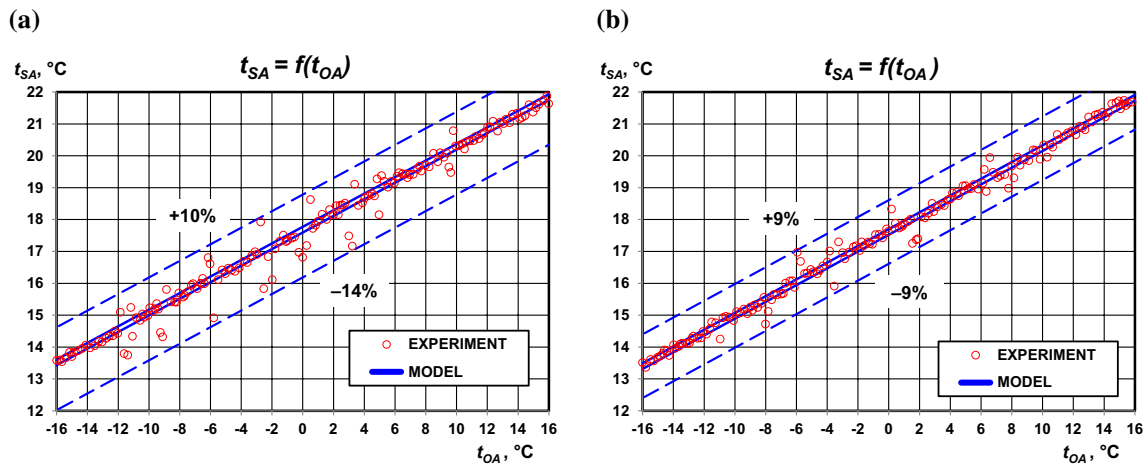


**Fig. 4** Selected results of model validation for the rotary heat exchanger: supply air temperature ( $t_{SA}$ ) expressed as a function of the outdoor air temperature ( $t_{OA}$ ) for air volumetric flow rate of

500 m<sup>3</sup>/h and two values of rotor speed: **a** 12 revolution per minute and **b** 16 revolution per minute

are presented on the charts (Figs. 5, 6, 7, 8, 9, 10, 11, 12, 13, 14) for each variant.

On the basis of the chart (Fig. 5) it can be seen that within the considered range of outdoor air temperature different zones of heat and mass transfer may be formed on the rotor’s surface: “dry,” “wet” and “frost.” As one can see, “dry” area dominates at higher values of  $t_{1i}$ ; however, as the outdoor air temperature drops, share of this area’s surface decreases at the expense of the rest of the zones. An opposite trend is observed when “frost” area is analyzed—the colder air is supplied to the heat exchanger,

the larger surface is covered by frost. Moreover, within a certain range of sub-zero outdoor air temperature  $t_{1i} = (-20 \dots -10.7) \text{ }^\circ\text{C}$ , the increase in the wheel’s heat recovery efficiency is noted, what can be explained as the effect of released heat of phase transition. It is also worth noting that “frost” area is additionally divided into two sub-zones, which distinguish the area with frost accumulation from the other one, where frost is molten as a result of the contact with the warmer air stream. It allows to indicate the important range of temperature  $t_{1i} = (-10.7 \dots -5) \text{ }^\circ\text{C}$ , in which the whole formed frost melts down. For the outdoor

**Fig. 5** The percentage distribution of different heat and mass transfer zones inside the rotary heat exchanger expressed as a function of outdoor air temperature values supplemented by the effectiveness of the device (for return air parameters:  $t_{2i} = 20 \text{ }^\circ\text{C}$ ,  $RH_{2i} = 40\%$  and rotor depth 0.20 m)

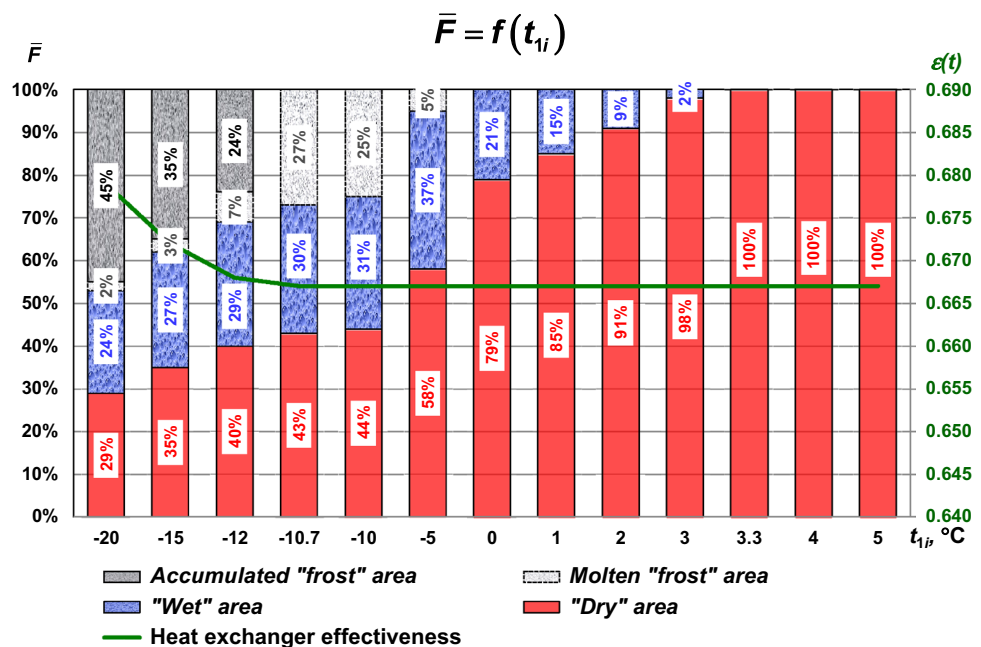


**Fig. 6** Two water–vapor mass transfer rates inside outdoor and return air heat exchanger sides expressed as a function of outdoor air temperature values (for return air parameters:  $t_{2i} = 20\text{ }^\circ\text{C}$ ,  $\text{RH}_{2i} = 40\%$  and rotor depth 0.20 m)

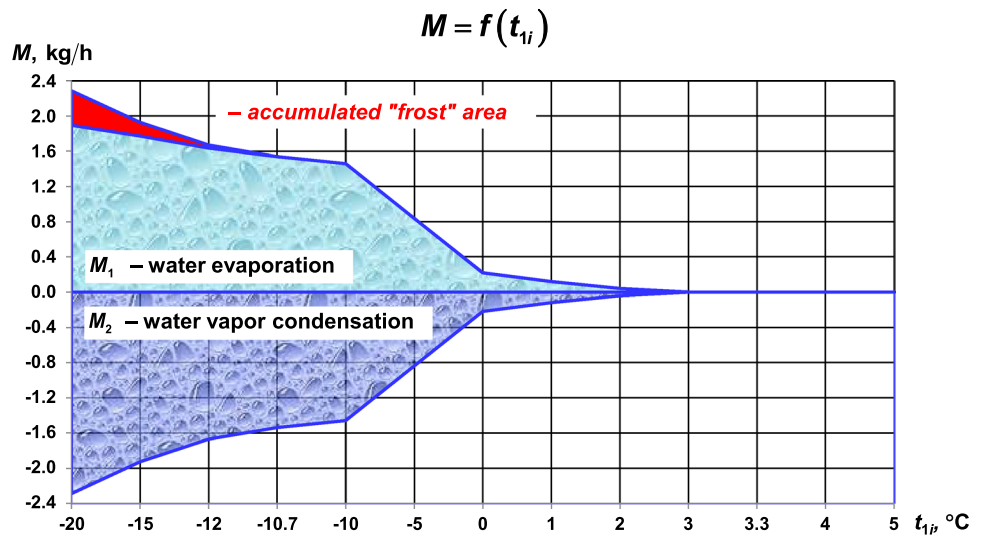
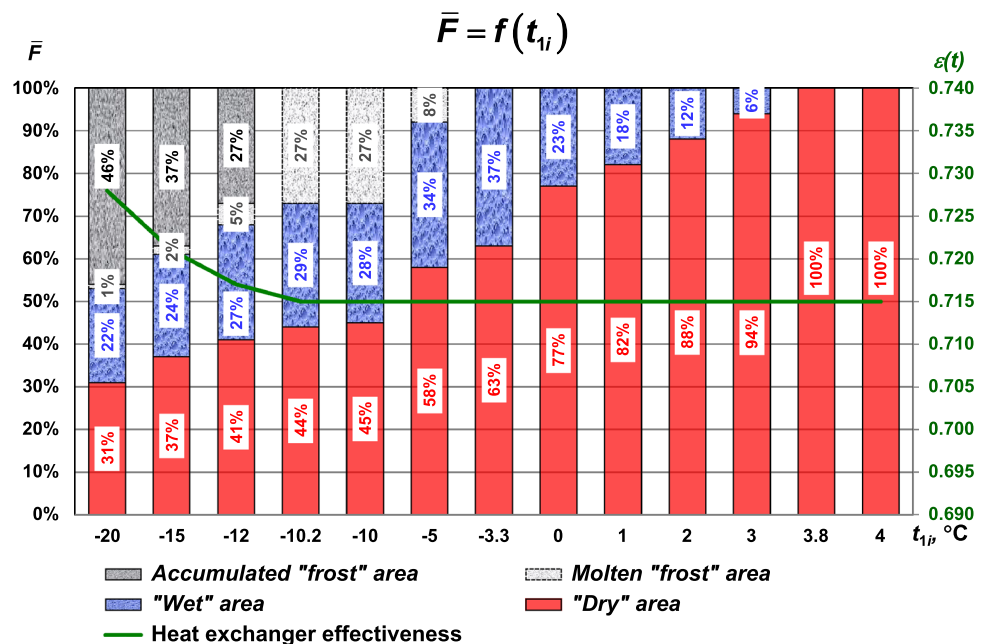


**Fig. 7** The percentage distribution of different heat and mass transfer zones inside the rotary heat exchanger expressed as a function of outdoor air temperature values supplemented by the effectiveness of the device (for return air parameters:  $t_{2i} = 20\text{ }^\circ\text{C}$ ,  $\text{RH}_{2i} = 40\%$  and rotor depth 0.25 m)



air temperature  $t_{1i} < -10.7\text{ }^\circ\text{C}$ , the process of frost accumulation begins. At the same time, molten “frost” area gradually decreases. The single most striking issue to emerge from the analysis of Fig. 5 is the variability of the temperature effectiveness of heat recovery depending on the values of the outdoor air temperature. For the conditions of “dry” heat exchange  $t_{1i} = (3.3 \dots 5)\text{ }^\circ\text{C}$ , the lack of significant changes in the effectiveness of the exchanger seems obvious. On the other hand, with the decrease in outdoor air temperature  $t_{1i} < 3.3\text{ }^\circ\text{C}$ , heat of phase transition is released, what can be observed in a form of the “wet” area. Despite the favorable phenomenon of condensation, the temperature effectiveness of the thermal wheel remains constant. The explanation of this result

is the mass balance on the both sides of rotor  $M_1 = M_2$  (Fig. 6). This condition stays unchanged up to the threshold temperature  $t_{1i} = -10.7\text{ }^\circ\text{C}$ . On the left-hand side of this value, the process of frost accumulation begins due to the mass disbalance  $M_1 < M_2$ . Therefore, the increase in the temperature effectiveness of the heat exchanger (Fig. 5) should be attributed to the excess mass rate of condensed water–vapor which occurs on the return air side  $M_2$  (Fig. 6). This effect is extremely noticeable within the range of outdoor air temperature  $t_{1i} = (-20 \dots -10.7)\text{ }^\circ\text{C}$ .

The exact variability in the effectiveness of rotary heat exchanger may be observed by analyzing both mass rates of condensed and evaporated water inside two airflow sections (Fig. 6). On the basis of this graph,

**Fig. 8** Two water–vapor mass transfer rates inside outdoor and return air heat exchanger sides expressed as a function of outdoor air temperature values (for return air parameters:  $t_{2j} = 20\text{ }^\circ\text{C}$ ,  $\text{RH}_{2j} = 40\%$  and rotor depth 0.25 m)

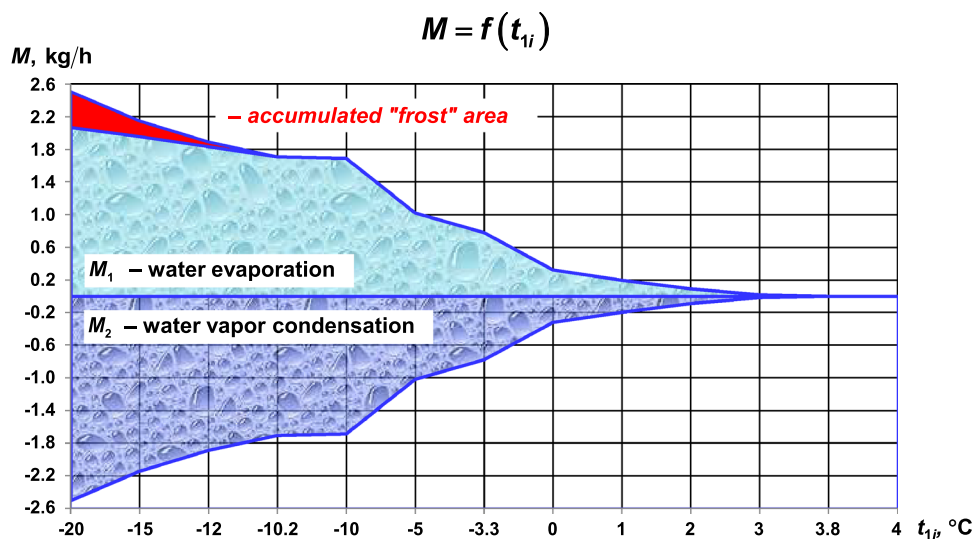
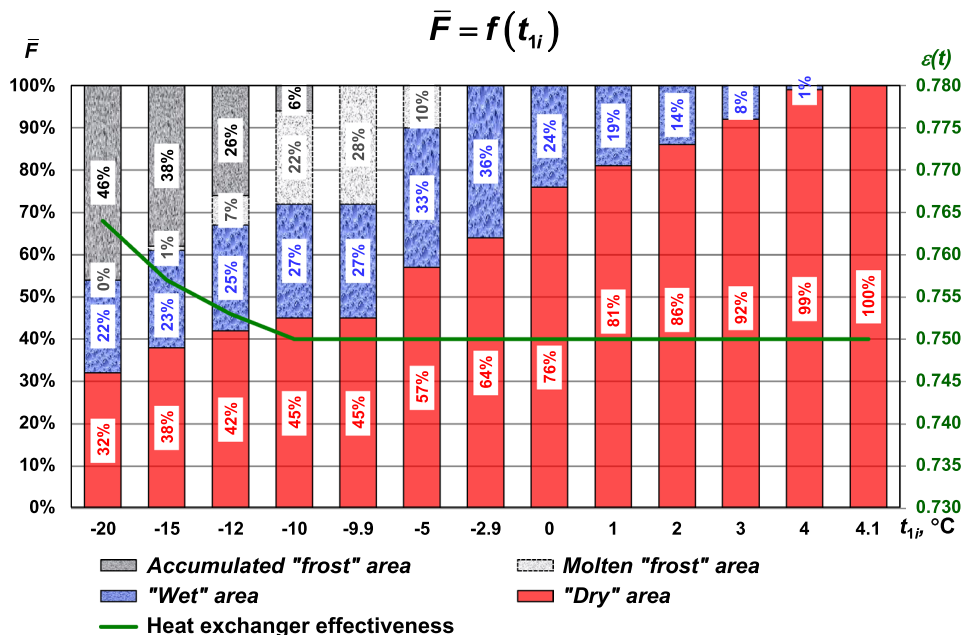


**Fig. 9** The percentage distribution of different heat and mass transfer zones inside the rotary heat exchanger expressed as a function of outdoor air temperature values supplemented by the effectiveness of the device (for return air parameters:  $t_{2j} = 20\text{ }^\circ\text{C}$ ,  $\text{RH}_{2j} = 40\%$  and rotor depth 0.30 m)



it is possible to pick out three particular heat and mass transfer modes: lack of mass transfer  $t_{1j} = (3.3 \dots 5)\text{ }^\circ\text{C}$ , balanced mass transfer  $t_{1j} = (-10.7 \dots 3.3)\text{ }^\circ\text{C}$  and disbalanced mass transfer (frost accumulation)  $t_{1j} = (-20 \dots -10.7)\text{ }^\circ\text{C}$ . Only within the third range of outdoor air temperature, the latent heat released during the process of condensation of water–vapor is partially taken during the evaporation of water in the adjacent channel and the rest of this heat is used for additional heating of the wheel matrix. As a result, the supply air stream temperature rises what leads directly to the increase in the temperature effectiveness of heat recovery.

The results of numerical simulations for the rest variants of rotor’s width were conducted in the same form (Figs. 7, 8, 9, 10, 11, 12, 13, 14).

On the basis of the presented charts (Figs. 5, 6, 7, 8, 9, 10, 11, 12, 13, 14), one can notice that the function of the temperature effectiveness is shaped in a similar way for all presented variants of the rotor’s depth, i.e., its value rises due to moisture accumulation (in the form of water film or frost layer). Another similarity is an increase in “dry” area with increasing outdoor air temperature. Moreover, the influence of the rotor’s size on the heat and mass transfer process is also observed. The most noticeable relationship is an increase in the temperature effectiveness of heat recovery as the geometrical parameters of

**Fig. 10** Two water–vapor mass transfer rates inside outdoor and return air heat exchanger sides expressed as a function of outdoor air temperature values (for return air parameters:  $t_{2i} = 20\text{ }^\circ\text{C}$ ,  $\text{RH}_{2i} = 40\%$  and rotor depth 0.30 m)

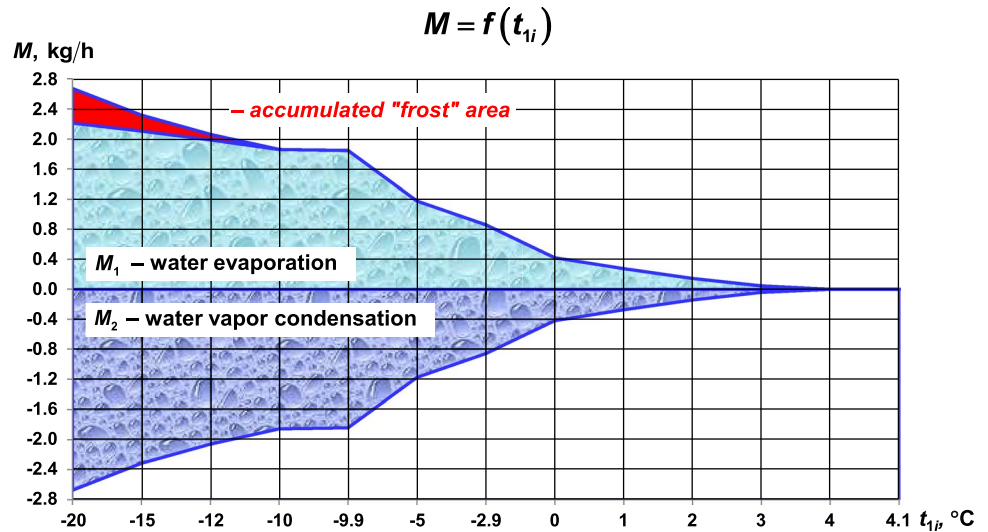
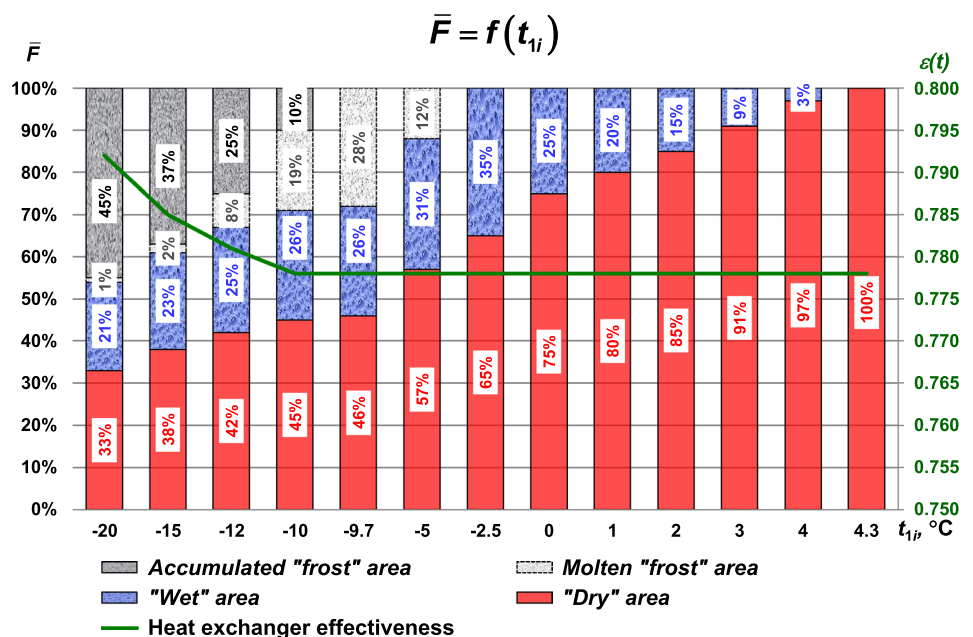


**Fig. 11** The percentage distribution of different heat and mass transfer zones inside the rotary heat exchanger expressed as a function of outdoor air temperature values supplemented by the effectiveness of the device (for return air parameters:  $t_{2i} = 20\text{ }^\circ\text{C}$ ,  $\text{RH}_{2i} = 40\%$  and rotor depth 0.35 m)



the wheel rise. The next conclusion is concerned with the formation of different heat and mass transfer zones. On the one hand, larger depth of the rotor causes an increase in “wet” area on the surface of the storage mass. On the other hand, for the lowest values of outdoor air temperature within the range of  $t_{1i} = (-20 \dots -10)\text{ }^\circ\text{C}$  the total area covered with both “wet” and “frost” zones is greater for the smaller depth of the rotary heat exchanger. The influence of the wheel’s depth is also visible analyzing the values of threshold outdoor air temperature, at which frost accumulation begins inside the channels. It turns out that there is a clear trend of increasing frosting limit temperature by raising the rotor’s depth. In case of outdoor air temperature  $t_{1i} = -10\text{ }^\circ\text{C}$ , while operating the wheel

with a depth of 0.20 m, there is no accumulated “frost” area. For the same outdoor air temperature, the largest size of the rotor causes 10% of accumulated “frost” zone. Another important conclusion is that increasing depth of the wheel ensures the release of much larger latent heat.

The main limitation of operation of these types of regenerators is a possibility of frost building up on the inlet supply air side of the heat exchanger (Fig. 2). Unfortunately, such issues can only be analyzed by means of numerical simulations with the use of programs developed on the basis of mathematical models. Effective testing of rotary heat exchanger operation in freezing conditions is very dangerous because it can cause permanent damage or even destruction of unit. For this reason, future

**Fig. 12** Two water–vapor mass transfer rates inside outdoor and return air heat exchanger sides expressed as a function of outdoor air temperature values (for return air parameters:  $t_{2i} = 20\text{ }^\circ\text{C}$ ,  $\text{RH}_{2i} = 40\%$  and rotor depth 0.35 m)

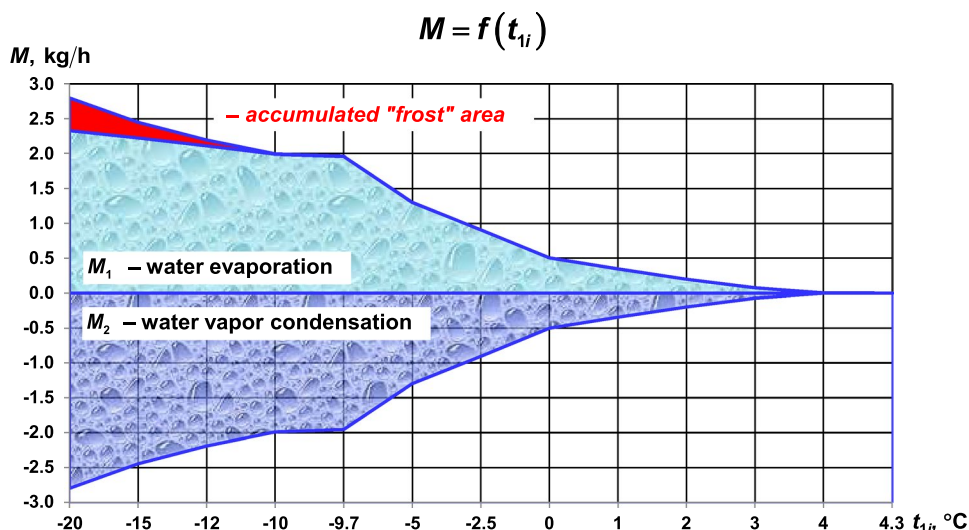
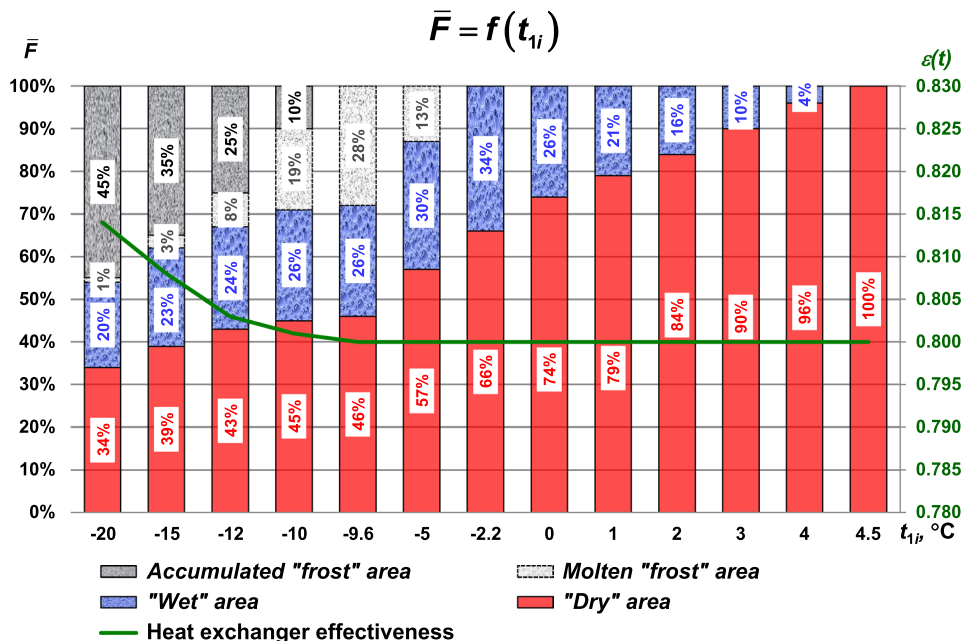


**Fig. 13** The percentage distribution of different heat and mass transfer zones inside the rotary heat exchanger expressed as a function of outdoor air temperature values supplemented by the effectiveness of the device (for return air parameters:  $t_{2i} = 20\text{ }^\circ\text{C}$ ,  $\text{RH}_{2i} = 40\%$  and rotor depth 0.40 m)



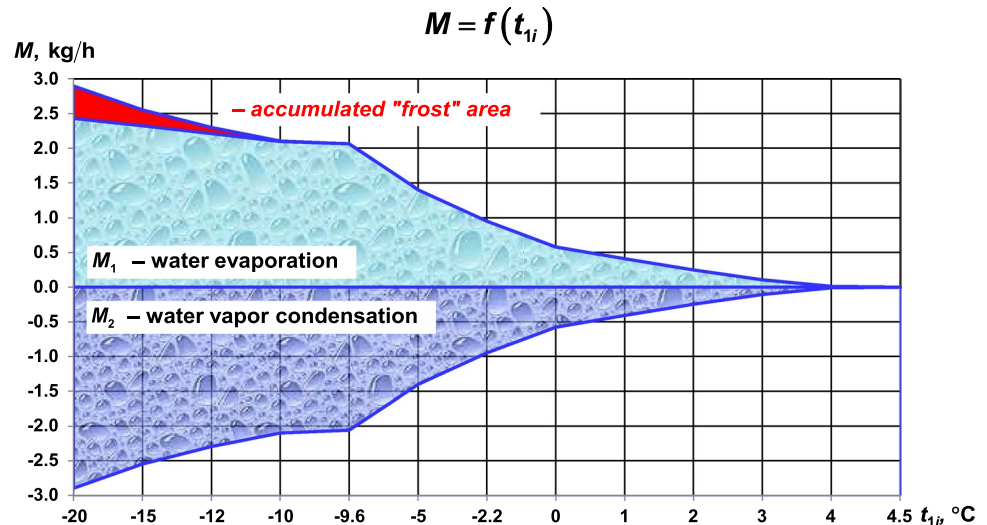
directions of research will be carried out in order to determine the inlet air parameters for safe operation of the heat exchanger. In the next stages, the possibilities of reducing the effectiveness of the device will be analyzed, which, as could be seen in the graphs (Figs. 5, 6, 7, 8, 9, 10, 11, 12, 13, 14), allow for the elimination of frost accumulation zones, causing its melting.

## 6 Conclusions

In this paper, the influence of geometrical parameters of a rotary heat exchanger on heat and mass transfer processes as well as its temperature effectiveness is investigated.

For this purpose, the mathematical model of a heat recovery wheel based on a structure of the counter-flow heat exchanger model was developed. It can be used successfully when high-speed rotor conditions are considered. The next step was to implement a numerical method that could be used to solve developed heat and mass transfer balance equations, and afterward the computer simulations were carried out. As a result, the percentage distribution of different heat and mass transfer zones inside the wheel as a function of outdoor air temperature value for various rotor depths was presented. Furthermore, the analysis of the water–vapor mass transfer between supply and return air sides of the heat exchanger was conducted. It constitutes a fundamental

**Fig. 14** Two water–vapor mass transfer rates inside outdoor and return air heat exchanger sides expressed as a function of outdoor air temperature values (for return air parameters:  $t_{2i} = 20$  °C,  $RH_{2i} = 40\%$  and rotor depth 0.40 m)



explanation of the variability of the temperature effectiveness with outdoor air temperature change.

Presented analysis allowed to receive the following conclusions:

- It was indicated that moisture accumulation has a significant influence on the increase in temperature effectiveness of heat recovery. This property is a result of the released heat of phase transition, which in the cases under consideration means an increase in efficiency of 1.4%.
- Rotary heat exchangers equipped with a larger rotor are characterized by a higher limit temperature, which determines the occurrence of condensation (in the case of rotor depth equal to 0.20 m  $\rightarrow t_{1i} < 3.3$  °C but for the rotor depth equal 0.40 m  $\rightarrow t_{1i} < 4.5$  °C).
- The increase in rotor's depth leads to the increase in temperature effectiveness of the rotary heat exchanger (from 0.667 to 0.814) because of larger heat and mass transfer area. This effect is observed under both "dry" and "wet" heat transfer conditions. The geometrical parameters of the wheel have also the influence on the frost accumulation threshold temperature—the value of temperature increases with increasing of the rotor's depth (from  $-10.7$  to  $-9.6$  °C) (a deeper rotor causes a greater cooling of the return air stream, which in turn causes the surface temperature of the wheel matrix to fall below 0 °C and the dew point temperature to drop faster).
- It was also shown that the total area of both "frost" and "wet" zones under conditions of the extremely low values of the outdoor air temperature  $t_{1i} = (-20 \dots -10)$  °C is in the range (66...55)% and is smaller than for a smaller depth of rotor (71...56)%.

The received results will be the basis for further optimization studies, and they will allow evaluating the possibility of using a rotary heat exchanger depending on climatic conditions.

**Acknowledgements** This work was supported by The Faculty of Environmental Engineering, Wrocław University of Science and Technology, Poland (No. 0401/0055/18).

### Compliance with ethical standards

**Conflict of interest** The authors declare that they have no conflict of interest.

**Open Access** This article is distributed under the terms of the Creative Commons Attribution 4.0 International License (<http://creativecommons.org/licenses/by/4.0/>), which permits unrestricted use, distribution, and reproduction in any medium, provided you give appropriate credit to the original author(s) and the source, provide a link to the Creative Commons license, and indicate if changes were made.

### References

1. Pérez-Lombard L, Ortiz J, Pout C (2008) A review on buildings energy consumption information. *Energy Build* 40:394–398. <https://doi.org/10.1016/j.enbuild.2007.03.007>
2. Allouhi A, El Fouih Y, Kousksou T, Jamil A, Zeraouli Y, Mourad Y (2015) Energy consumption and efficiency in buildings: current status and future trends. *J Clean Prod* 109:118–130. <https://doi.org/10.1016/j.jclepro.2015.05.139>
3. Logachev KI, Ziganshin AM, Averkova OA, Logachev AK (2018) A survey of separated airflow patterns at inlet of circular exhaust hoods. *Energy Build* 173:58–70. <https://doi.org/10.1016/j.enbuild.2018.05.036>
4. ASHRAE (2004) Air-to-air energy recovery. In: Owen MS (ed) ASHRAE handbook 2004: HVAC systems and equipment, Atlanta

5. Mardiana-Idayu A, Riffat SB (2012) Review on heat recovery technologies for building applications. *Renew Sustain Energy Rev* 16:1241–1255. <https://doi.org/10.1016/j.rser.2011.09.026>
6. KLINGENBURG. Quick guide 2018: Rotors overview. <http://www.klingenburg.uk/downloads/all-documents/>. Accessed 20 Jan 2019
7. HOVAL. Rotary heat exchangers for heat recovery in ventilation systems: handbook for design, installation and operation. <http://www.hoval-entventus.com/en/products-and-solutions/downloads/>. Accessed 20 Jan 2019
8. Sparrow EM, Tong JCK, Johnson MR, Martin GP (2007) Heat and mass transfer characteristics of a rotating regenerative total energy wheel. *Int J Heat Mass Transf* 50:1631–1636. <https://doi.org/10.1016/j.ijheatmasstransfer.2006.07.035>
9. Holmberg RB (1989) Prediction of condensation and frosting limits in rotary wheels for heat recovery in buildings. *ASHRAE Trans* 95:64–69
10. Nizovtsev MI, Borodulin VY, Letushko VN (2017) Influence of condensation on the efficiency of regenerative heat exchanger for ventilation. *Appl Therm Eng* 111:997–1007. <https://doi.org/10.1016/j.applthermaleng.2016.10.016>
11. Anisimov S, Jedlikowski A, Pandelidis D (2015) Frost formation in the cross-flow plate heat exchanger for energy recovery. *Int J Heat Mass Transf* 90:201–217. <https://doi.org/10.1016/j.ijheatmasstransfer.2015.06.056>
12. Jedlikowski A, Anisimov S, Danielewicz J, Karpuk M, Pandelidis D (2017) Frost formation and freeze protection with bypass for counter-flow recuperators. *Int J Heat Mass Transf* 108:585–613. <https://doi.org/10.1016/j.ijheatmasstransfer.2016.12.047>
13. Justo Alonso M, Liu P, Mathisen HM, Ge G, Simonson CJ (2015) Review of heat/energy recovery exchangers for use in ZEBs in cold climate countries. *Build Environ* 84:228–237. <https://doi.org/10.1016/j.buildenv.2014.11.014>
14. Fathieh F, Besant RW, Evitts RW, Simonson CJ (2015) Determination of air-to-air heat wheel sensible effectiveness using temperature step change data. *Int J Heat Mass Transf* 87:312–326. <https://doi.org/10.1016/j.ijheatmasstransfer.2015.04.028>
15. Abe OO, Simonson CJ, Besant RW, Shang W (2006) Effectiveness of energy wheels from transient measurements. Part I: prediction of effectiveness and uncertainty. *Int J Heat Mass Transf* 49:52–62. <https://doi.org/10.1016/j.ijheatmasstransfer.2005.08.002>
16. Abe OO, Simonson CJ, Besant RW, Shang W (2006) Effectiveness of energy wheels from transient measurements: part II—results and verification. *Int J Heat Mass Transf* 49:63–77. <https://doi.org/10.1016/j.ijheatmasstransfer.2005.08.009>
17. Simonson CJ, Besant RW (1999) Energy wheel effectiveness: part I—development of dimensionless groups. *Int J Heat Mass Transf* 42:2161–2170. [https://doi.org/10.1016/S0017-9310\(98\)00325-1](https://doi.org/10.1016/S0017-9310(98)00325-1)
18. Simonson CJ, Besant RW (1999) Energy wheel effectiveness: part II—correlations. *Int J Heat Mass Transf* 42:2171–2185. [https://doi.org/10.1016/S0017-9310\(98\)00327-5](https://doi.org/10.1016/S0017-9310(98)00327-5)
19. Seo J-W, Lee D-Y, Kim D-S (2018) A simple effectiveness model for heat wheels. *Int J Heat Mass Transf* 120:1358–1364. <https://doi.org/10.1016/j.ijheatmasstransfer.2017.12.102>
20. Büyükalaca O, Yilmaz T (2002) Influence of rotational speed on effectiveness of rotary-type heat exchanger. *Heat Mass Transf* 38:441–447. <https://doi.org/10.1007/s002310100277>
21. Kays WM, London AL (1984) Compact heat exchangers, 3rd edn. McGraw-Hill, New York
22. Bilodeau S, Brousseau P, Lacroix M, Mercadier Y (1999) Frost formation in rotary heat and moisture exchangers. *Int J Heat Mass Transf* 42:2605–2619. [https://doi.org/10.1016/S0017-9310\(98\)00323-8](https://doi.org/10.1016/S0017-9310(98)00323-8)
23. Rafati Nasr M, Fauchoux M, Besant RW, Simonson CJ (2014) A review of frosting in air-to-air energy exchangers. *Renew Sustain Energy Rev* 30:538–554. <https://doi.org/10.1016/j.rser.2013.10.038>
24. Pacak A, Jedlikowski A, Karpuk M, Anisimov S (2019) Analysis of power demand calculation for freeze prevention methods of counter-flow heat exchangers used in energy recovery from exhaust air. *Int J Heat Mass Transf* 133:842–860. <https://doi.org/10.1016/j.ijheatmasstransfer.2018.12.144>
25. Liu P, Rafati Nasr M, Ge G, Justo Alonso M, Mathisen HM, Fathieh F, Simonson CJ (2016) A theoretical model to predict frosting limits in cross-flow air-to-air flat plate heat/energy exchangers. *Energy Build* 110:404–414. <https://doi.org/10.1016/j.enbuild.2015.11.007>
26. Liu P, Justo Alonso M, Mathisen HM, Simonson CJ (2016) Performance of a quasi-counter-flow air-to-air membrane energy exchanger in cold climates. *Energy Build* 119:129–142. <https://doi.org/10.1016/j.enbuild.2016.03.010>
27. Liu P, Mathisen HM, Justo Alonso M, Simonson CJ (2017) A frosting limit model of air-to-air quasi-counter-flow membrane energy exchanger for use in cold climates. *Appl Therm Eng* 111:776–785. <https://doi.org/10.1016/j.applthermaleng.2016.10.010>
28. Jedlikowski A, Anisimov S (2017) Analysis of the frost formation and freeze protection with bypass for cross-flow recuperators. *Appl Therm Eng* 116:731–765. <https://doi.org/10.1016/j.applthermaleng.2017.01.105>
29. Bogoslovsky VN, Poz MY (1983) Fundamentals of physics of heating, ventilation and air-conditioning units design. Stroyisdat, Moscow (**in Russian**)
30. Bogoslovsky VN, Poz MY (1984) Thermal physics of heat exchangers for HVAC systems. Stroyisdat, Moscow (**in Russian**)
31. Holmberg RB (1989) Sensible and latent heat transfer in cross-counterflow gas-to-gas heat exchanger. *ASME J Heat Transf* 111:173–177
32. Shah RK, London AL (1978) Laminar flow forced convection in ducts. Supplement 1 to advances in heat transfer. Academic Press, New York
33. Shah RK, Sekulić DP (2003) Fundamentals of heat exchanger design. Wiley, Hoboken
34. Hasselgreaves JE, Law R, Reay DA (2017) Compact heat exchangers. Selection, design and operation, 2nd edn. Butterworth-Heinemann, Oxford
35. Rohsenow WM, Hartnett JP, Cho YI (1998) Handbook of heat transfer, 3rd edn. McGraw-Hill, New York
36. Žukauskas A, Žiugžda J (1969) Heat transfer in laminar flow of fluid. Mintis, Vilnius (**in Russian**)
37. Lykov AV (1980) Heat and mass transfer. MiR Publishers, Distributed by Imported Publications, Moscow
38. Yilmaz T, Büyükalaca O (2003) Design of regenerative heat exchangers. *Heat Transf Eng* 24:32–38. <https://doi.org/10.1080/01457630304034>
39. Ikeda K, Fujino Ch, Yamauchi Y (1977) Heat and mass transfer in the nonisothermal fixed bed adsorption column with nonlinear equilibrium. *Bull Fac Eng Yokohama Natl Univ* 26:117–139
40. Jedlikowski A (2012) Heat transfer in cross flow heat exchangers for heat recovery from exhaust air in ventilation and air conditioning systems. Dissertation, Wrocław University of Technology
41. Patankar SV (1980) Numerical heat transfer and fluid flow. Hemisphere Publishing Corporation, Washington

**Publisher's Note** Springer Nature remains neutral with regard to jurisdictional claims in published maps and institutional affiliations.